Supplementary Information (SI) for Journal of Materials Chemistry C.

Supporting Information

Significant Self-Heating Effect in High-Power High-Speed Organic Field-Effect Transistor Arrays

Boxin Hao, Qingkai Chen, Shu Zhang, Yang Li, Boyu Peng*, and Hanying Li*

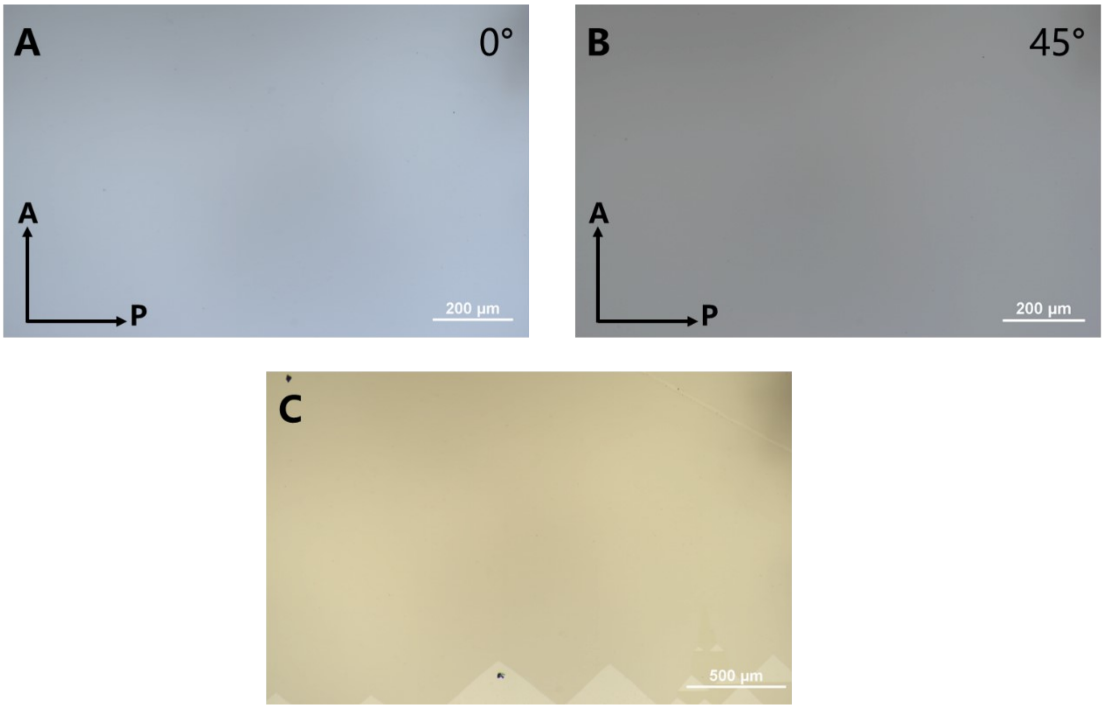

Fig. S1 A, B) POM images of monolayer crystals grown on Al_2O_3/Si substrate. The black arrows indicate the directions of the polarizer and analyzer. The degree in the upper right corner indicates the angle between the polarization direction and the crystal growth direction. C) POM image of the large area molecular monolayer crystal film grown on Al_2O_3/Si substrate.

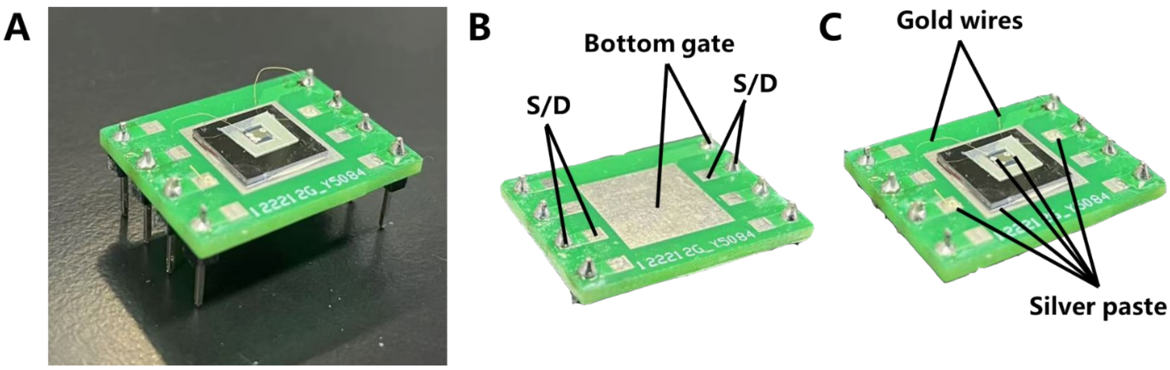

Fig. S2 Custom PCB (A) to connect devices and circuit, and how it works (B, C).

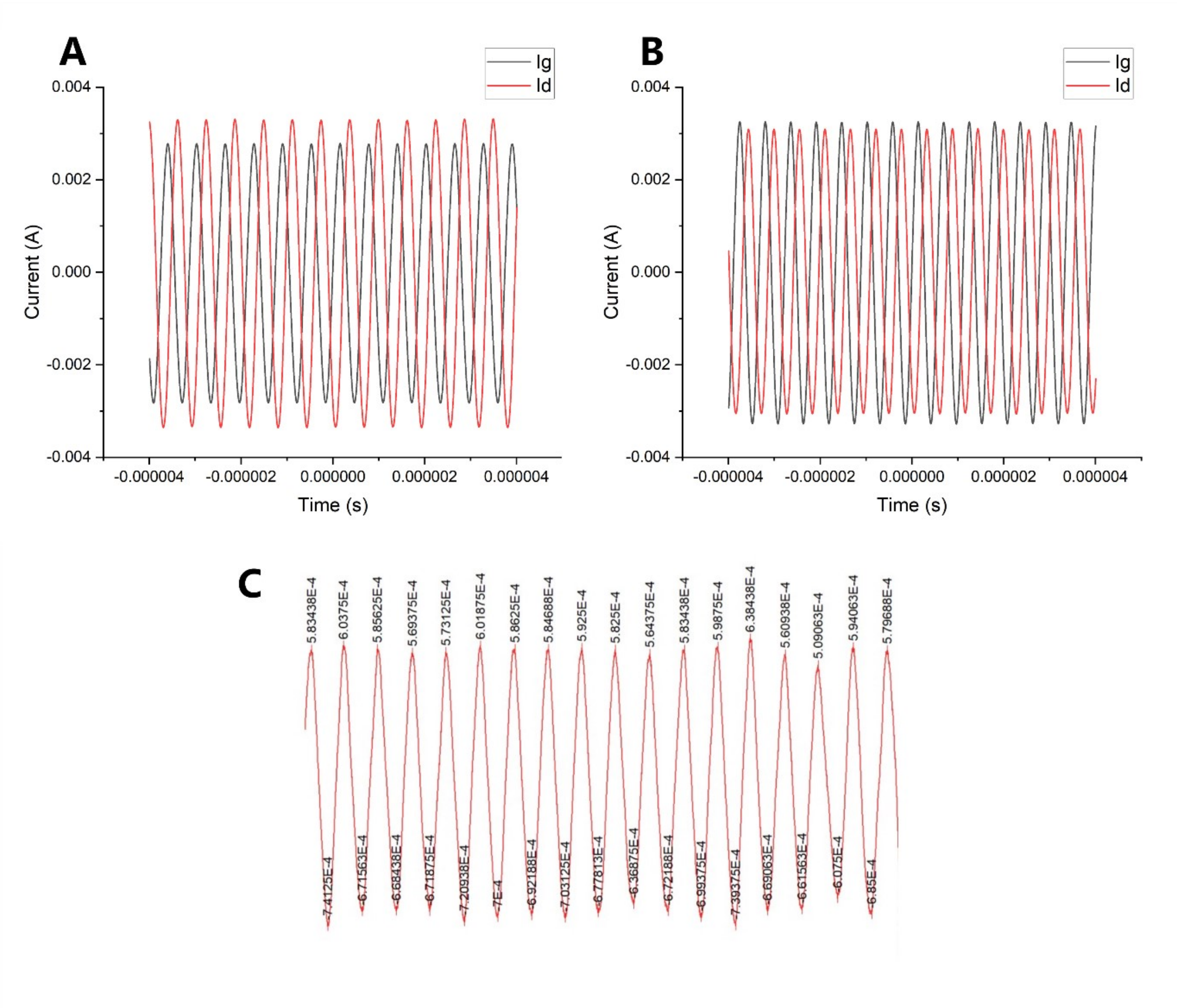

Fig. S3 The method to obtain the gain of high-speed operating devices. A) The waveform of I_g and I_d of a device that has not reached f_T, the amplitude of I_d (A_{Id}) is larger than the amplitude of Ig (A_{Ig}). B) The waveform of I_g and Id of a device that has not reached f_T, the amplitude of I_d (A_{Id}) is smaller than the amplitude of I_g (A_{Ig}). The gain is defined as $\log(A_{Id}/A_{Ig})$. C) The extraction of the amplitudes.

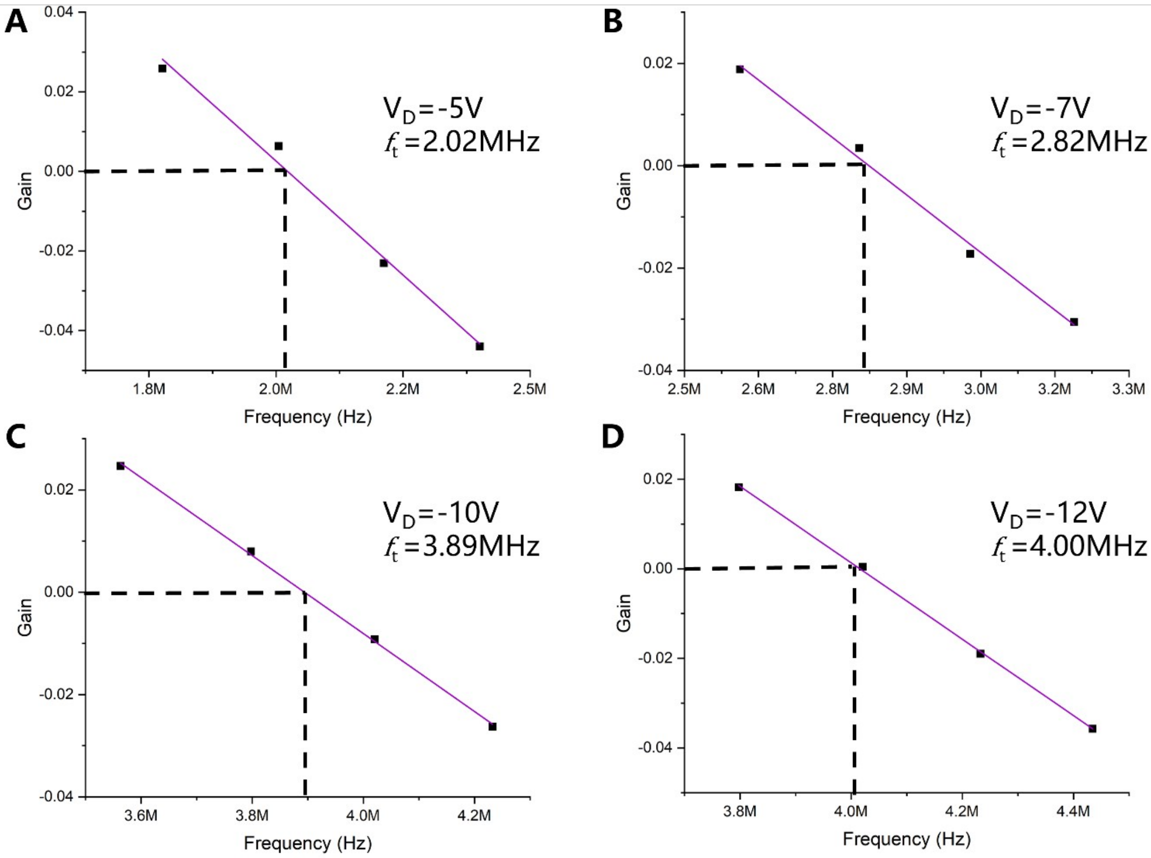

Fig. S4 The estimation of the f_T of the device on SiO_2/Si substrate at different V_d.

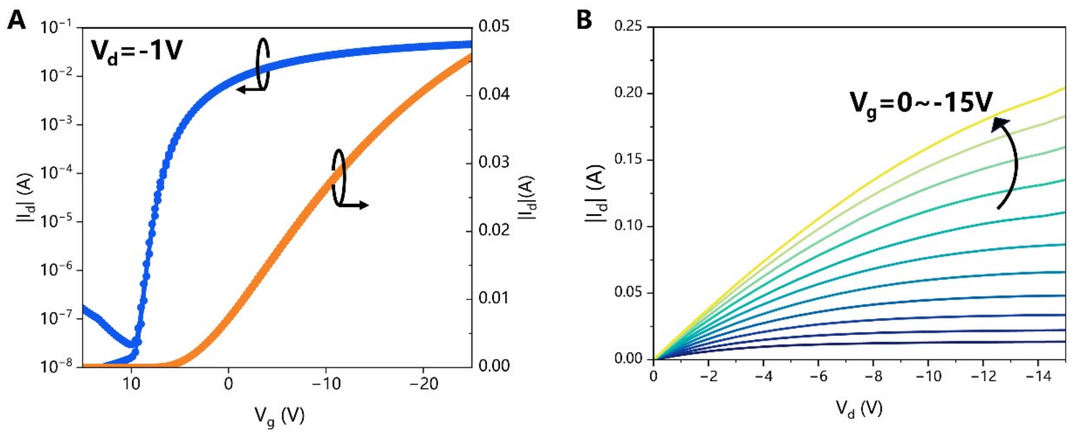

Fig. S5 The transfer and output curves of the multi-finger OFET array on Al_2O_3/Si substrate.

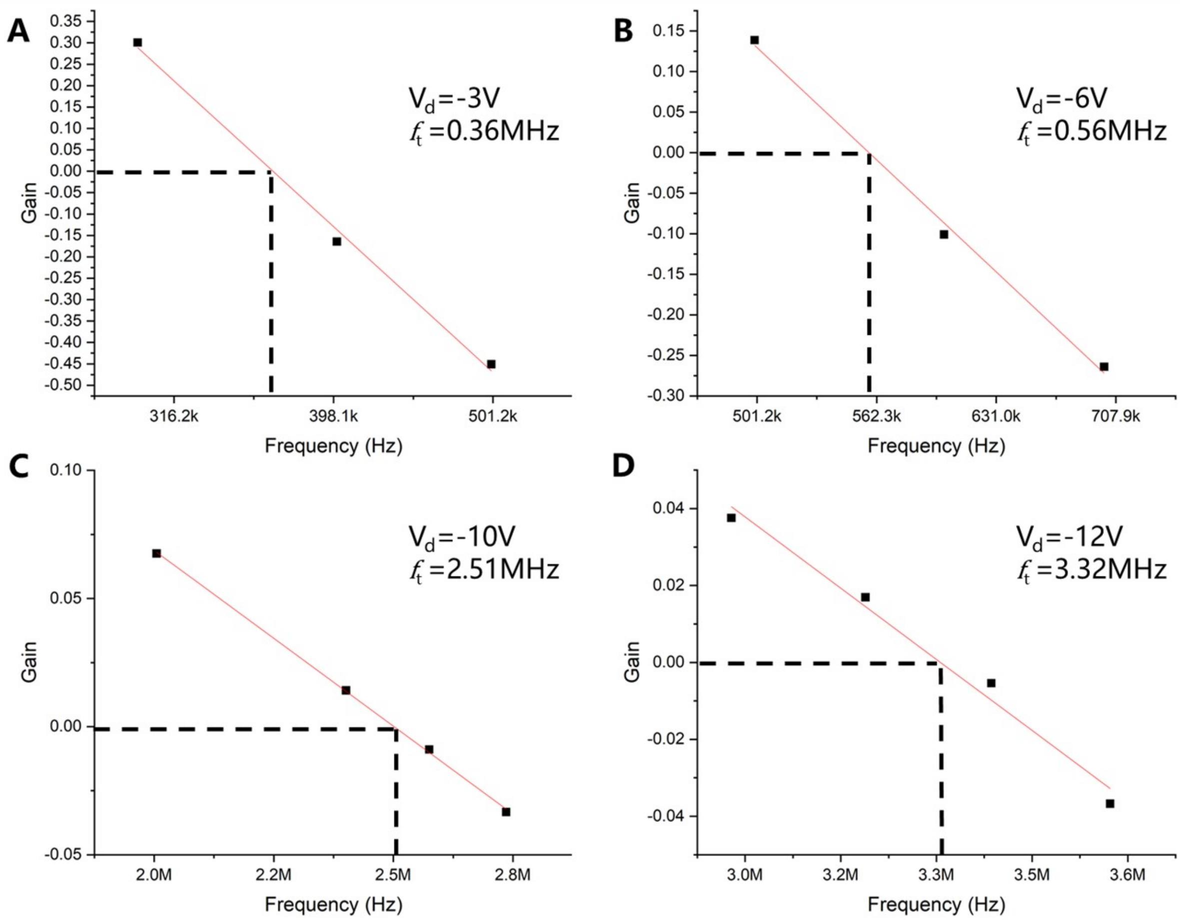

Fig. S6 The estimation of the f_T of the device on Al_2O_3/Si substrate at different V_d.

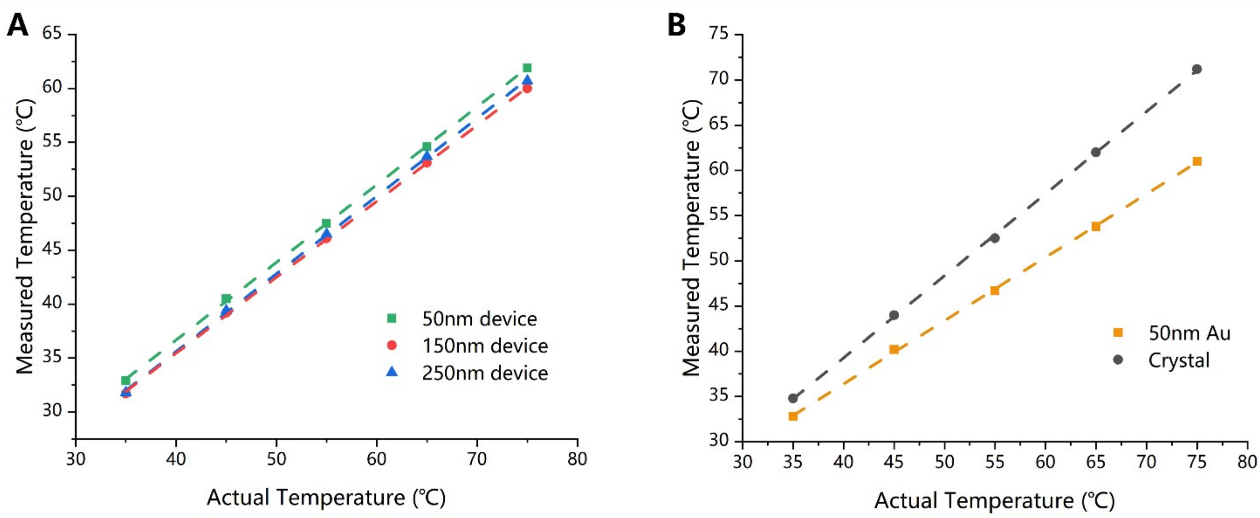

Fig. S7 The calibration of thermal imaging by measuring known temperatures of A) overall device area with different electrode thicknesses, B) 50 nm Au electrodes and semiconductor crystals (channels).

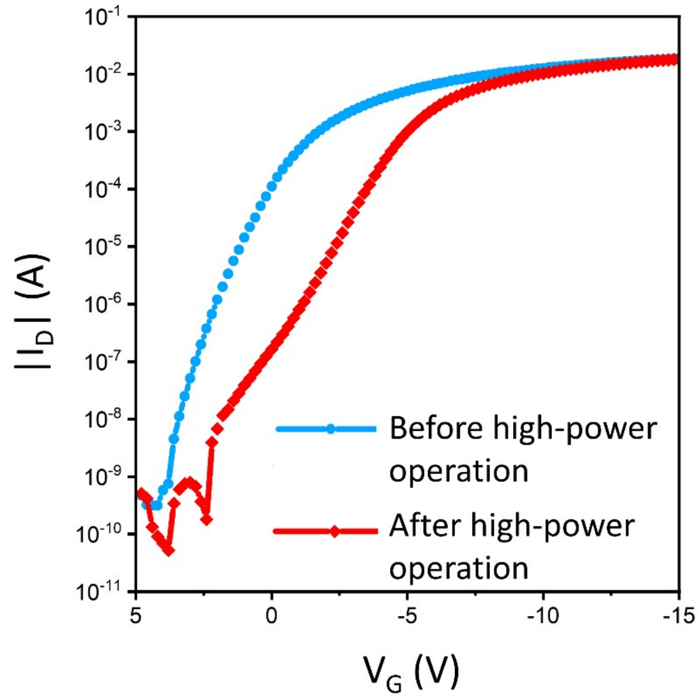

Fig. S8 The abnormal changes of transfer curves in the test performed immediately after the bias stress.

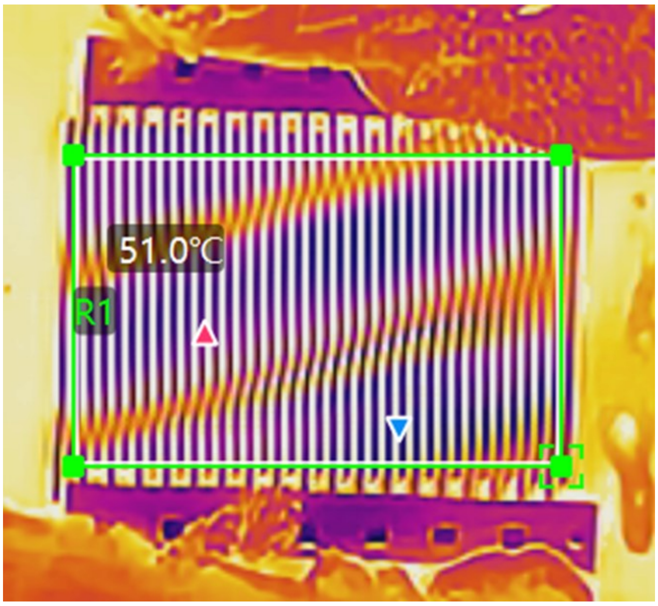

Fig. S9 The temperature distribution of a long-channel device.

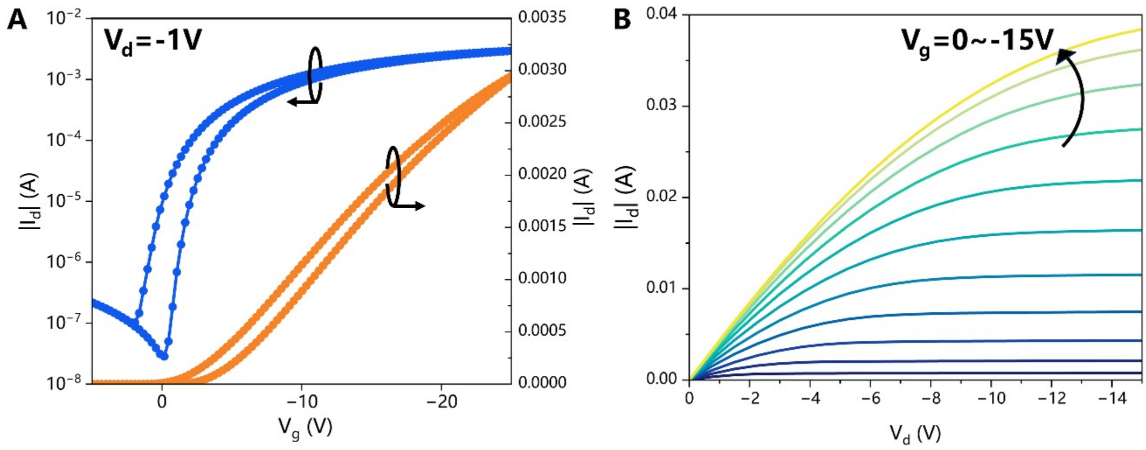

Fig. S10 The transfer and output curves of the multi-finger OFET array with 10 fingers.

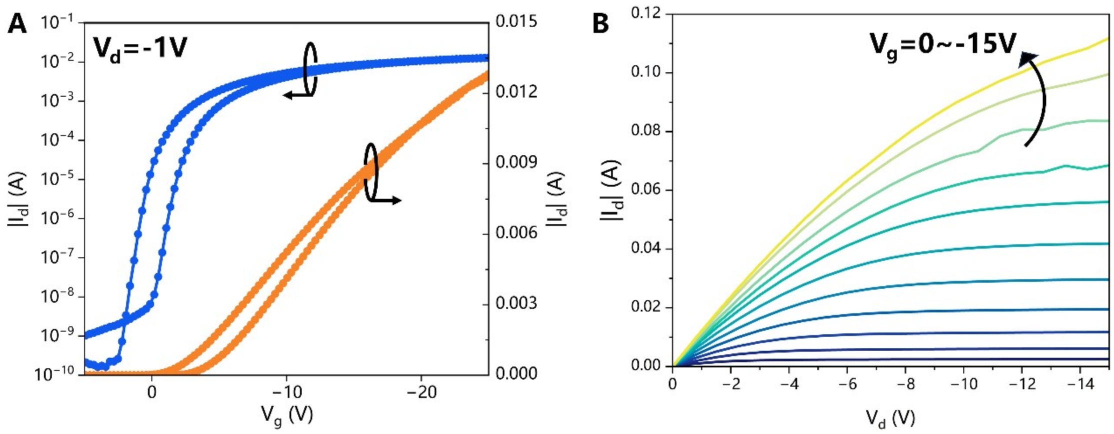

Fig. S11 The transfer and output curves of the multi-finger OFET array with 80 fingers.

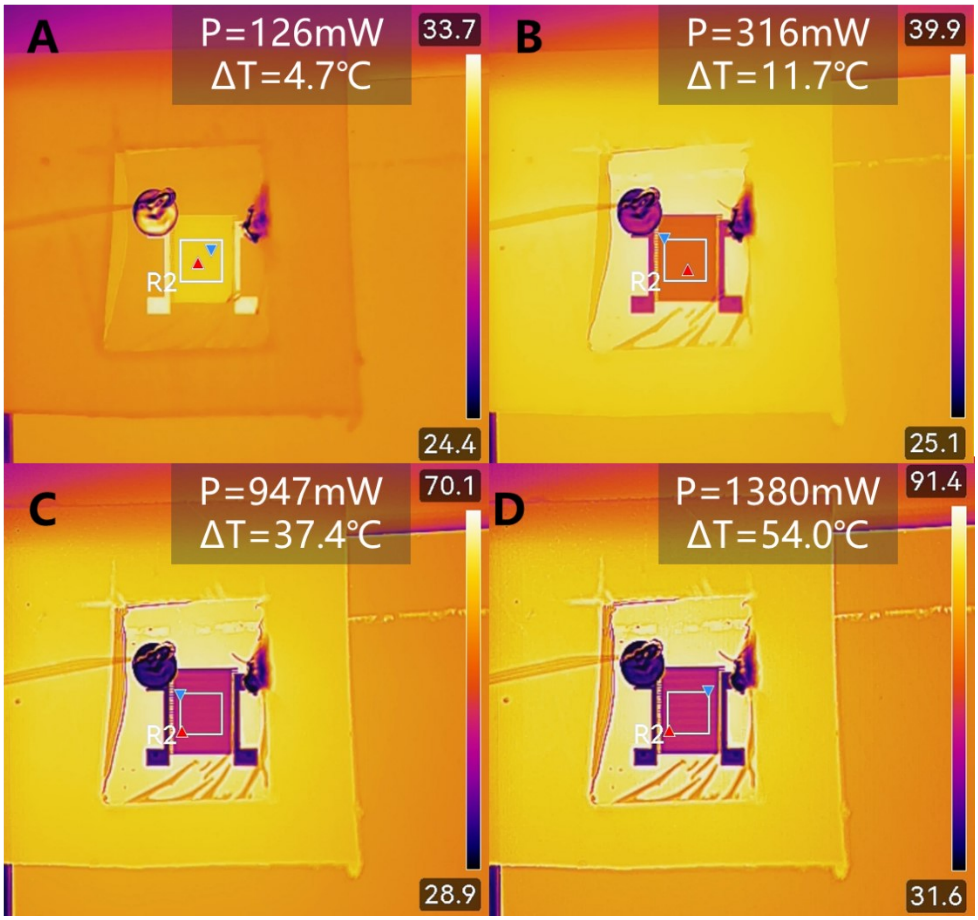

Fig. S12 IR thermal images of the multi-finger OFET array with 150 nm thick electrodes under bias stress with corresponding power (*P*) and temperature rise (*ΔT*).

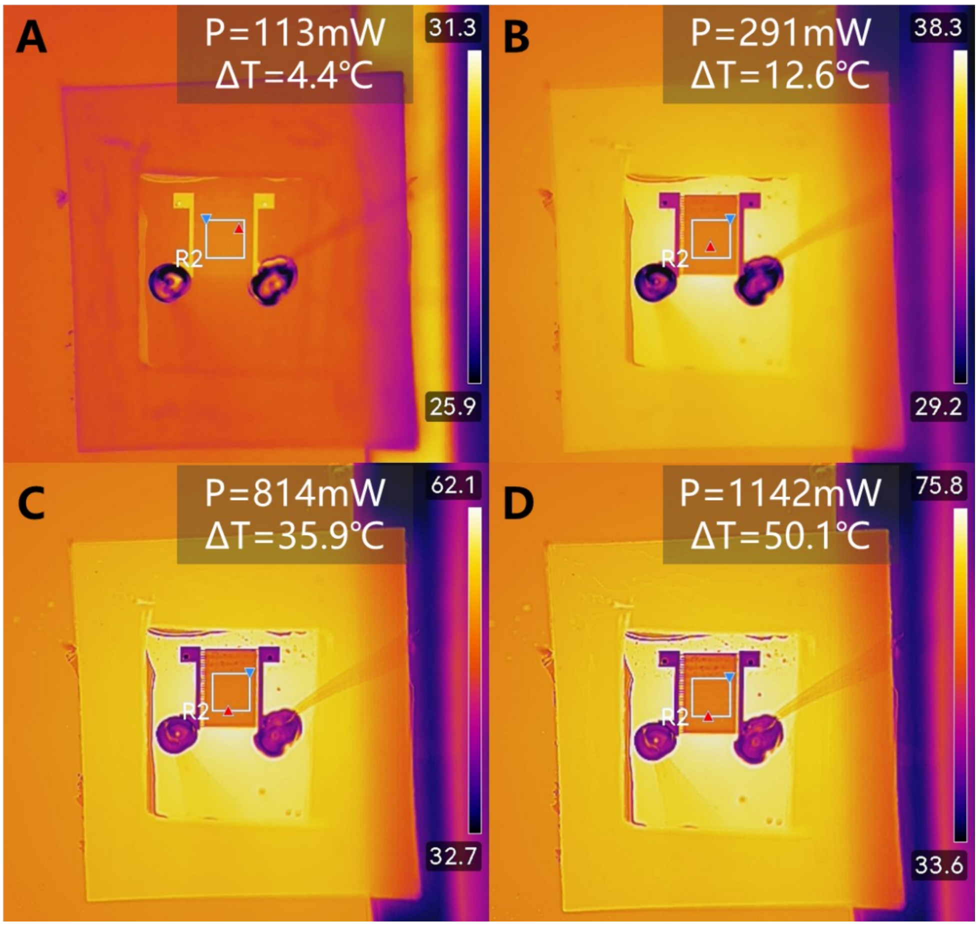

Fig. S13 IR thermal images of the multi-finger OFET array with 250 nm thick electrodes under bias stress with corresponding power (*P*) and temperature rise (*ΔT*).

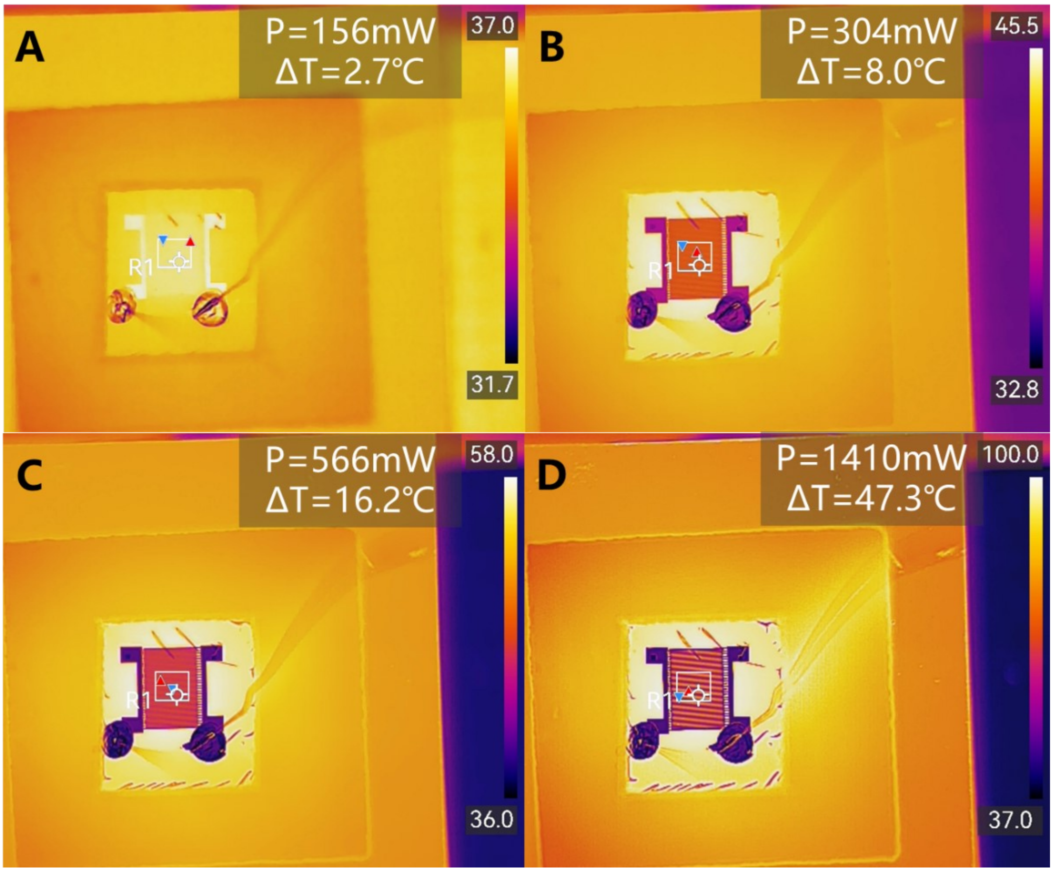

Fig. S14 IR thermal images of the multi-finger OFET array on Al_2O_3/Si substrate under bias stress with corresponding power (*P*) and temperature rise (*ΔT*).

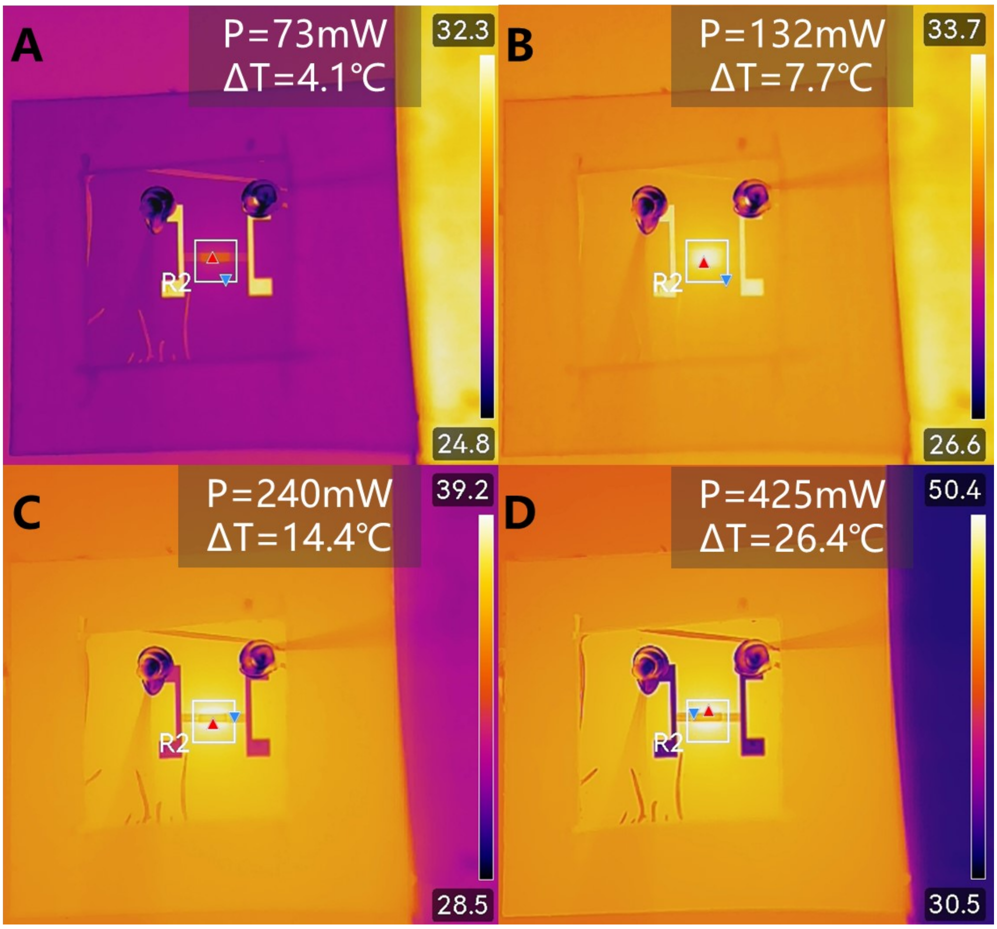

Fig. S15 IR thermal images of the multi-finger OFET array with 10 fingers under bias stress with corresponding power (*P*) and temperature rise (*ΔT*).

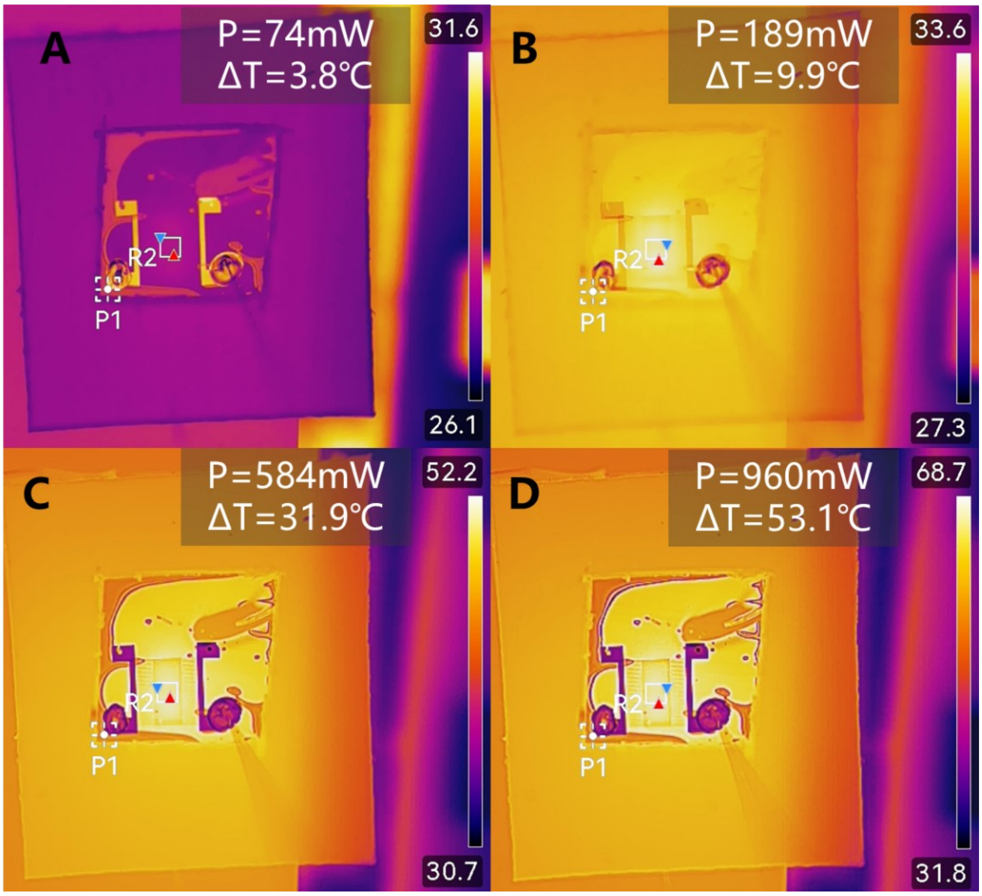

Fig. S16 IR thermal images of the multi-finger OFET array with 80 fingers under bias stress with corresponding power (*P*) and temperature rise (*ΔT*).

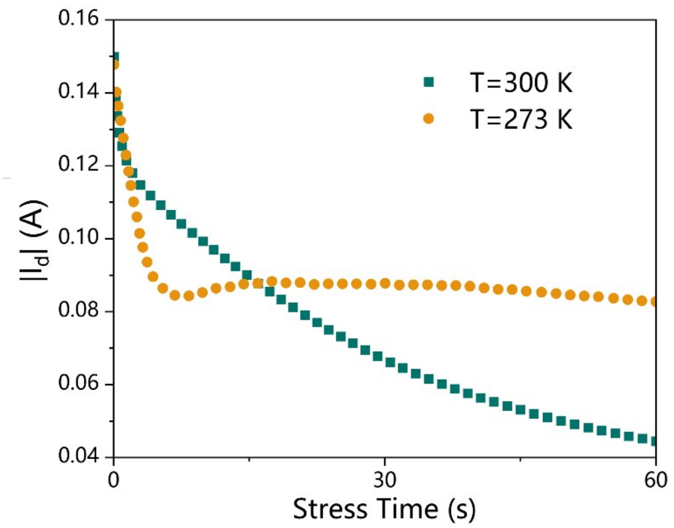

Fig. S17 The bias stress I_d degradation of OFET array at room temperature (300 K) and low ambient temperature (273 K).

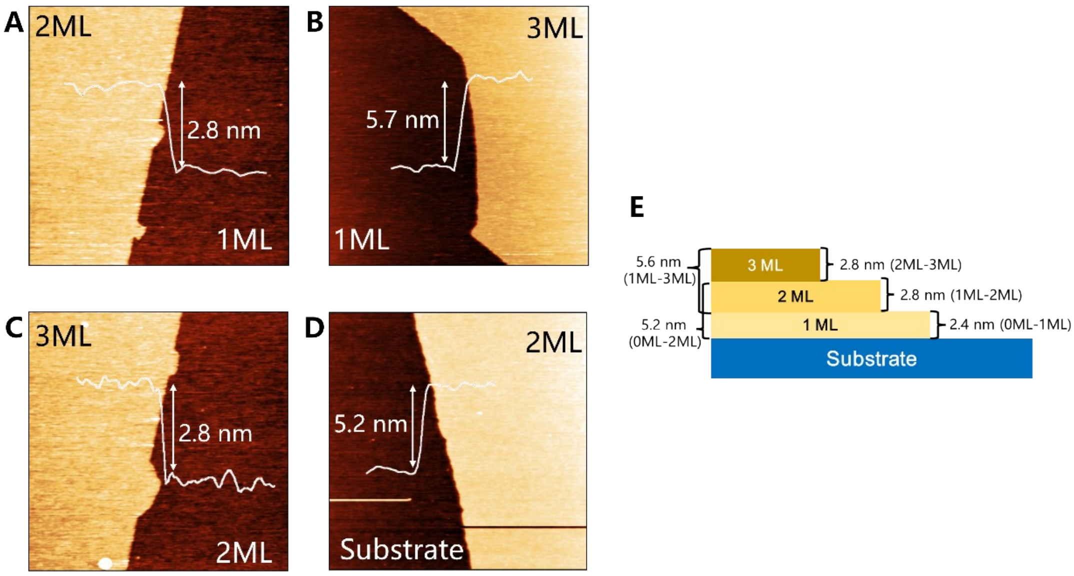

Fig. S18 The images of AFM step height measurement at the edge of (A) 1ML-2ML, (B) 1ML-3ML, (C) 2ML-3ML, (D) substrate (0ML)-2ML.

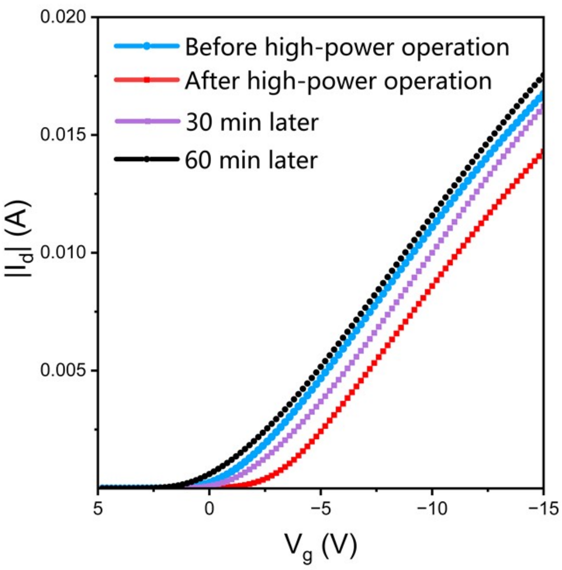

Fig. S19 The reversibility of abnormal changes of transfer curves in the test performed immediately after the bias stress.

Table S1 Summary of power and power density for the devices in this work and previously reported high-power OFET devices

References	L (μm)	W (μm)	A (cm^2)	P_{0max} (W/cm^2)	P_{max} (W)
46	20	1000	0.0002	1280	0.256
47	40	8.7	3.48×10^{-6}	457	0.00159
48	50	1400	0.0007	400	0.280
49	50	1000	0.0005	424	0.212
50	80	1000	0.0008	153	0.122
51	100	500	0.0005	200	0.100
52	40	1400	0.00056	709	0.397
53	4.4	5	2.2×10^{-7}	7052	0.00155
54	50	1000	0.0005	125	0.0625
55	20	1000	0.0002	117	0.0234
56	20	10000	0.002	36	0.0720
57	40	200	0.00008	44.5	0.00356
This work	6.5	89890	0.0058	414.8	2.41
This work	10	40000	0.004	273.8	1.10
This work	12	5000	0.0006	802.5	0.482
This work	6.5	89890	0.0058	527.6	3.06

References

46 H.-R. Tseng, L. Ying, B. B. Y. Hsu, L. A. Perez, C. J. Takacs, G. C. Bazan and A. J. Heeger, *Nano Lett.*, 2012, **12**, 6353–6357.
47 H. Li, B. C.-K. Tee, J. J. Cha, Y. Cui, J. W. Chung, S. Y. Lee and Z. Bao, *J. Am. Chem. Soc.*, 2012, **134**, 2760–2765.
48 A. Zhang, C. Xiao, Y. Wu, C. Li, Y. Ji, L. Li, W. Hu, Z. Wang, W. Ma and W. Li, *Macromolecules*, 2016, **49**, 6431–6438.
49 J. Lee, A.-R. Han, H. Yu, T. J. Shin, C. Yang and J. H. Oh, *J. Am. Chem. Soc.*, 2013, **135**, 9540–9547.
50 H. Tseng, H. Phan, C. Luo, M. Wang, L. A. Perez, S. N. Patel, L. Ying, E. J. Kramer, T. Nguyen, G. C. Bazan and A. J. Heeger, *Adv. Mater.*, 2014, **26**, 2993–2998.
51 H. Iino, T. Usui and J. Hanna, *Nat. Commun.*, 2015, **6**, 6828.
52 Y. Ji, C. Xiao, Q. Wang, J. Zhang, C. Li, Y. Wu, Z. Wei, X. Zhan, W. Hu, Z. Wang, R. A. J. Janssen and W. Li, *Adv. Mater.*, 2016, **28**, 943–950.
53 V. K. Bandari, Y. Gu, S. Shi, Y. Nan, K. He, Y. Li, N. Bandari, S. Moradi, H. Tian, F. Zhu, Y. Geng, D. Yan and O. G. Schmidt, *Adv. Funct. Mater.*, 2019, **29**, 1903738.
54 G. Giri, E. Verploegen, S. C. B. Mannsfeld, S. Atahan-Evrenk, D. H. Kim, S. Y. Lee, H. A. Becerril, A. Aspuru-Guzik, M. F. Toney and Z. Bao, *Nature*, 2011, **480**, 504–508.
55 M. Nikolka, I. Nasrallah, B. Rose, M. K. Ravva, K. Broch, A. Sadhanala, D. Harkin, J. Charmet, M. Hurhangee, A. Brown, S. Illig, P. Too, J. Jongman, I. McCulloch, J.-L. Bredas and H. Sirringhaus, *Nat. Mater.*, 2017, **16**, 356–362.
56 M. P. Hein, A. A. Zakhidov, B. Lüssem, J. Jankowski, M. L. Tietze, M. K. Riede and K. Leo, *Appl. Phys. Lett.*, 2014, **104**, 013507.
57 H. F. Iqbal, Q. Ai, K. J. Thorley, H. Chen, I. McCulloch, C. Risko, J. E. Anthony and O. D. Jurchescu, *Nat. Commun.*, 2021, **12**, 2352.